Computational Study of Astroglial Calcium Homeostasis in a Semi-isolated Synaptic Cleft

Marinus Toman
Computational Neuroscience and Neural Engineering Research Team (CNET), Intelligent Systems Research Centre (ISRC)
School of Computing, Engineering and Intelligent Systems, Ulster University
Derry, United Kingdom
toman-m1@ulster.ac.uk

John Joseph Wade
Computational Neuroscience and Neural Engineering Research Team (CNET), Intelligent Systems Research Centre (ISRC)
School of Computing, Engineering and Intelligent Systems, Ulster University
Derry, United Kingdom
https://orcid.org/0000-0003-1300-9429

Liam McDaid
Computational Neuroscience and Neural Engineering Research Team (CNET), Intelligent Systems Research Centre (ISRC)
School of Computing, Engineering and Intelligent Systems, Ulster University
Derry, United Kingdom
https://orcid.org/0000-0002-1197-4375

Jim Harkin
Computational Neuroscience and Neural Engineering Research Team (CNET), Intelligent Systems Research Centre (ISRC)
School of Computing, Engineering and Intelligent Systems, Ulster University
Derry, United Kingdom
https://orcid.org/0000-0001-7484-8205

***Abstract*—Astrocytes can affect neuronal communication by controlling extracellular ionic concentration levels. In the hippocampus, astrocytes have an intimate relationship with neuronal synapses, enwrapping the synapse tightly to prevent chemical diffusion between synapses, a phenomenon known as semi-isolated synapses. Calcium (Ca^{2+}) is known to enhance neurotransmitter release at excitatory synapses and release is dependent on levels of Ca^{2+} in the perisynaptic environment. Astrocytes have a great influence on Ca^{2+} levels at semi-isolated synapses, thus, they can affect neuronal transmission through control of synaptic Ca^{2+} levels. The perisynaptic astrocytic processes that semi-isolate synapses are exceedingly thin, typically having a diameter less than 100nm, therefore, these processes are most likely devoid of intracellular organelles and therefore, Ca^{2+} stores. Astrocytes possess many transmembrane proteins that can traffic Ca^{2+} into and out of the cell, with the plasma membrane ATPase and the sodium/calcium exchanger being the main transporters capable of carrying Ca^{2+} across the plasma membrane in large quantities.**

The main aim of this research is to capture a more complete astroglial Ca^{2+} pathway as this may be important for understanding biological processes involving Ca^{2+} such as synaptic transmission, plasticity and ultimately learning. We use a computational approach to capture the ionic dynamics in a semi-isolated synapse, with particular focus on Ca^{2+} dynamics. The model presented here is an extension of a recently published model that hypothesises the formation of Ca^{2+} microdomains in perisynaptic astrocytes. We take this hypothesis further and show that these Ca^{2+} microdomains can act as a local supply of Ca^{2+} to the synaptic cleft during periods of sustained excitability.

Keywords—dynamic astrocyte-neuron model, astrocyte-neuron interactions, neuronal excitability, calcium signalling, computational model, mathematical model

I. INTRODUCTION

Astrocytes are a sub-type of glial cell in the mammalian brain that provides a variety of roles in the central nervous system (CNS) including molecular homeostasis and neuronal structural support. It was once thought that glial cells only provided supporting roles for neurons, however, recent evidence suggests they can contribute to information processing in the brain through influencing the points of information transfer; neuronal synapses [1]. Astrocytes are the most abundant glial cell in the brain and they are sub-divided into broad types, the most common being protoplasmic astrocytes [2]. Protoplasmic astrocytes cover up to 80% of neuronal synapses in the hippocampus, which is an area of the brain believed to be important for memory formation [3], [4]. Protoplasmic astrocytes can "sense" neuronal activity at synapses they cover and take action to facilitate or inhibit synaptic transmission by changing concentration levels of signalling molecules in the synaptic environment [5]. It is currently very difficult to perform experiments on extremely thin astroglial processes, therefore, modelling is an important tool for capturing cellular ion dynamics [6], [7], and this is the approach used in this work. As protoplasmic astrocytes can affect synaptic transmission through homeostasis, they are the focus of this work and they will be referred to as astrocytes hereafter. It has been proposed that astrocytes semi-isolate synapses they cover, preventing molecules or ions diffusing away from or into the synaptic environment [3], this level of control of the synaptic environment suggests that dysfunctional astrocytes may be detrimental for healthy synapses and clear synaptic transmission. This research will assume the astrocyte enwraps the synapse tight enough to create a finite extracellular space for synaptic transmission to occur.

The calcium ion (Ca^{2+}) is a major signalling chemical in the mammalian CNS and is believed to be the primary substrate for astroglial signalling. Astrocytes can regulate

978-1-7281-6926-2/20/$31.00 ©2020 IEEE

concentration levels of Ca^{2+} in the CNS which consequently means they can influence biological processes that involve Ca^{2+}, including synaptic transmission and plasticity. Many experimental studies have reported propagating Ca^{2+} waves through astrocytes in response to neuronal activity, see [8] for a comprehensive review on astroglial glutamate uptake and signalling in the hippocampus. Despite an abundance of experimental evidence that shows astrocytes generate Ca^{2+} transients in response to neuronal excitability, the specific mechanisms by which these Ca^{2+} signals are generated is still under debate [8]. Organelles such as the endoplasmic reticulum are widely reported as intracellular stores of Ca^{2+} due to their large concentration relative to the cytosolic concentration [6]. It is thought that intracellular Ca^{2+} stores contribute significantly to Ca^{2+} waves in astrocytes, and indeed it has been shown that depletion of Ca^{2+} from the endoplasmic reticulum has the effect of diminishing Ca^{2+} wave magnitude, frequency and propagation [9], [10]. However, the spontaneous formation of local Ca^{2+} microdomains has been observed in distal astrocyte processes even after the intracellular stores are depleted and propagating waves have ceased [10], which may point to the formation of Ca^{2+} microdomains being independent of Ca^{2+} waves or intracellular stores. As the distal perisynaptic astrocyte processes are so thin, ~100 nm in diameter [11], we can assume there are no intracellular organelles in the perisynaptic region of the astrocyte (due to most organelles being wider than 100nm [4]) and hence there are no intracellular organelles in the present model.

Astrocytes express many transmembrane proteins necessary to maintain ionic homeostasis and often these proteins must translocate ions across the cellular membrane against their concentration gradients [2], e.g. the sodium-potassium ATPase (NKA) pumps sodium ions (Na^+) out of the cell and potassium ions (K^+) into the cell, both against their concentration gradients. The astrocytic transmembrane proteins considered in this work, shown in Fig. 1, include the excitatory amino acid transporter (EAAT), Na^+/Ca^{2+} exchanger (NCX), Na^+/K^+ ATPase (NKA), plasma membrane Ca^{2+} ATPase (PMCA), K^+ inward rectifying channel (Kir) and leak channels for each ionic species. The neuronal proteins considered include the NKA, PMCA, voltage-gated Ca^{2+}, Na^+ and K^+ channels and passive leak channels for each ion.

A recent model by [12] predicts the formation of Ca^{2+} microdomains in thin perisynaptic astrocyte processes due to the reversal of the sodium/calcium exchanger (NCX). It has been shown that a significant increase in cytosolic Na^+ can cause the NCX to enter reverse mode [12], and this causes the NCX to extrude Na^+ while allowing an influx of Ca^{2+}, which causes the formation of a Ca^{2+} microdomain. Here we build upon this model [12] and hypothesise that these predicted astroglial Ca^{2+} microdomains can serve as a local supply of Ca^{2+} to the synaptic cleft. By using only plasmalemmal channels, this work will show that these Ca^{2+} microdomains can act as a local supply of Ca^{2+} to the cleft.

II. Methods

A first-order mathematical framework is used to model the entire system, consisting of ordinary differential equations which describe the evolution of different parts of the system over time. The model presented builds upon a previous model which predicts the formation of Ca^{2+} microdomains in perisynaptic astrocyte processes due to the reversal of the NCX [12].

The presented astroglial homeostasis model is a five-compartment conductance-based model consisting of a presynaptic neuronal compartment (this compartment will be called Pre hereafter), a perisynaptic astrocyte compartment (called PsC hereafter), a synaptic cleft compartment (called ECS hereafter), an astrocytic soma (not shown in Fig. 1) and a global extracellular space compartment (GECS), see Fig. 1 for the schematic showing these compartments. The Pre and PsC compartments have various ionic channels and transporters embedded in their respective membranes, which are modelled using well established conductance-based equations. The well-mixed compartments in this model are the same as used in [12], [13], and contain Na^+, K^+ and Ca^{2+}. The model morphology is relatively simple, with cylindrical compartments used and assuming smooth surfaces.

The model presented in this paper is based around the concept of the tripartite synapse, which describes the communication between the neuronal synaptic cleft and perisynaptic astrocytic processes [14]. Usually, the tripartite synapse is used to explain astrocyte gliotransmission, the release of glutamate by the astrocyte to influence synaptic behaviour, however, as gliotransmission is still highly debated (see [15] and [16]), this research focuses on the astrocytic Ca^{2+} pathways which can influence synaptic behaviour. The astroglial ion channels and transporters

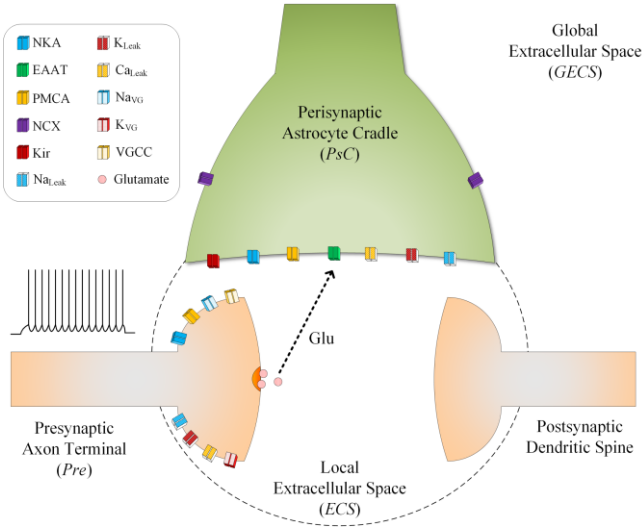

Fig. 1. Schematic showing ion channels and compartments of the homeostasis model. The astrocytic channels and their functions include the excitatory amino-acid transporter (EAAT) for glutamate clearance, the Na/K-ATPase (NKA) for Na^+/K^+ homeostasis, the Na/Ca exchanger (NCX) for Na^+/Ca^{2+} homeostasis, the K inward-rectifier (Kir) for K^+ homeostasis, the plasmalemma Ca-ATPase (PMCA) for Ca^{2+} homeostasis and leak currents for each ionic species which are used to balance the system at steady-state rest. Channels on the neuron include HH-type voltage-gated Na^+, K^+ and Ca^{2+} channels, a neuronal NKA and Na^+, K^+ and Ca^{2+} permeable leak channels. Compartments included in the model are the presynaptic neuron (Pre), the perisynaptic astrocyte cradle (PsC) and a finite local extracellular space (ECS). The postsynaptic neuron is not incorporated in the present model and only shown for illustration purposes, however, this cellular compartment will be studied in future work.

involved in trafficking Ca^{2+} across the plasma membrane are the PMCA and the NCX, both of which are sensitive to Ca^{2+} concentration changes [17], [18]. This work aims to capture a more complete astroglial Ca^{2+} signalling pathway.

The conventions used in the model follow modern conventions, i.e. transmembrane currents are denoted as negative for currents entering the cellular compartment, and positive for currents leaving the cell. To keep the modelling methodology consistent, the same modelling approach is employed for each compartment of the model, for example, the intracellular compartments consist of passive, active and voltage-gated (or neurotransmitter-gated) currents. The parameters are given in Table I and currents not described here are shown in Table II, with references to where the models are taken from.

A. Ionic Concentrations

The model consists of nine key variables which will control the state of the ionic concentrations of Ca^{2+}, Na^{+} and K^{+} in three of the five compartments; Pre, PsC and ECS. As the focus of the research is the ionic concentrations in the synaptic cleft, the concentrations are held constant in the GECS and astrocytic soma. Concentration changes are described in terms of transmembrane current produced by the electrogenic ion channels. Thus, the concentration changes in the model in Fig. 1 can be described by the following nine differential equations:

$$\frac{d[Ca^{2+}]_{ECS}}{dt} = -\left(\frac{ICa_{ECSDiff} - ICa_{VGCC} - ICa_{Ast}}{z_{Ca}FVol_{ECS}}\right) \quad (1)$$

$$\frac{d[Ca^{2+}]_{PsC}}{dt} = -\left(\frac{ICa_{Ast} + ICa_{NCX} + ICa_{PF}}{z_{Ca}FVol_{PsC}}\right) \quad (2)$$

$$\frac{d[Ca^{2+}]_{Pre}}{dt} = -\left(\frac{ICa_{Pre}}{z_{Ca}FVol_{Pre}}\right) \quad (3)$$

$$\frac{d[Na^{+}]_{ECS}}{dt} = -\left(\frac{INa_{ECSDiff} - INa_{Pre} - INa_{Ast}}{z_{Na}FVol_{ECS}}\right) \quad (4)$$

$$\frac{d[Na^{+}]_{PsC}}{dt} = -\left(\frac{INa_{Ast} + INa_{NCX} + INa_{PF}}{z_{Na}FVol_{PsC}}\right) \quad (5)$$

$$\frac{d[Na^{+}]_{Pre}}{dt} = -\left(\frac{INa_{Pre}}{z_{Na}FVol_{Pre}}\right) \quad (6)$$

$$\frac{d[K^{+}]_{ECS}}{dt} = -\left(\frac{IK_{ECSDiff} - IK_{Pre} - IK_{Ast}}{z_{K}FVol_{ECS}}\right) \quad (7)$$

$$\frac{d[K^{+}]_{PsC}}{dt} = -\left(\frac{IK_{Ast} + IK_{PF}}{z_{K}FVol_{PsC}}\right) \quad (8)$$

$$\frac{d[K^{+}]_{Pre}}{dt} = -\left(\frac{IK_{Pre}}{z_{K}FVol_{Pre}}\right) \quad (9)$$

Where $Ix_{ECSDiff}$ is the current generated through diffusion from the ECS to the GECS, Ix_{Ast} is the total astrocytic current, Ix_{NCX} is the NCX current, Ix_{PF} is the current generated down the astrocytic process, Ix_{Pre} is the total neuronal transmembrane current, x is the ion under consideration, z is the valency of each ion, F is Faraday's constant and Vol is the volume of each compartment.

B. Reversal Potential

The morphology used in this study is on a nanometer scale and we cannot assume the ionic concentrations will not change. As the concentrations change, the electrochemical driving force will change and we calculate this using the Nernst equation [7]:

$$E_x = \frac{RT}{z_x F} ln \frac{[x]_e}{[x]_i} \quad (10)$$

In this equation x is the ion under consideration, R is the ideal gas constant, T is the absolute temperature in Kelvin, z_x is the valency of x, F is Faraday's constant, $[x]_e$ is the extracellular concentration of ion x (relative to the compartment being considered) and $[x]_i$ is the intracellular concentration of ion x. All reversal potentials are calculated using (10).

C. Presynaptic Neuron

The presynaptic neuron is modelled using the standard HH formalism, with voltage-gated Na^{+} and K^{+} currents [19]. An extra high-threshold voltage-gated Ca^{2+} channel is added to the neuronal compartment to allow Ca^{2+} influx into the presynaptic neuron after an action potential [20]. The presynaptic neuron is stimulated with a variable current to produce a spike train, which has a predefined frequency.

1) Total Currents

The total currents in the neuronal compartment are a summation of voltage-gated currents, non-specific leak currents and concentration balancing currents, e.g. from the NKA pump that maintains large concentration gradients. The currents in the model are given as current densities and must be multiplied by the compartment surface areas to yield the actual currents. The total presynaptic neuronal currents are:

$$ICa_{Pre} = (ICa_{VGCC} + ICa_{PMCAPre} + ICa_{LPre})SA_{Pre}$$

$$INa_{Pre} = (INa_{VG} + INa_{NKAPre} + INa_{LPre})SA_{Pre}$$

$$IK_{Pre} = (IK_{VG} + IK_{NKAPre} + IK_{LPre})SA_{Pre}$$

Where ICa_{VGCC} is the current generated through the voltage-gated Ca^{2+} channel (VGCC), $ICa_{PMCAPre}$ is the PMCA current, Ix_{NKAPre} is the NKA current, Ix_{LPre} is the leak current, Ix_{VG} is the voltage-gated current, x is the ion under consideration, and SA_{Pre} is the surface area of the presynaptic neuronal compartment interacting with the ECS. The individual current densities in the model for INa_{VG} and IK_{VG} are taken from [19]. The only modification made to the model in [19] is that the reversal potentials are dynamic, this is a consequence of the small finite morphology used. Hodgkin and Huxley calculated that the membrane potential would change greatly from the movement of a relatively small number of ions, and they assumed that the change in ionic concentration was negligible as the intracellular volume was minuscule compared to the extracellular space volume, therefore, they assumed static reversal potentials. We do not assume the reversal potentials will remain constant at such small scales because ionic fluxes describe the number of ions crossing the membrane over a surface area, while ionic concentrations are proportional to volumes and, as mentioned, the volumes in the presented model are greatly reduced compared to [19].

2) Voltage-gated Calcium Current

The arrival of an action potential at the presynaptic terminal depolarises the cell membrane, leading to the opening VGCC's which allows an influx of Ca^{2+}. The rise of intracellular Ca^{2+} traffics synaptic vesicles to the presynaptic active zone to be primed for exocytosis. The high-threshold

P/Q-type VGCC's have been shown to participate in synaptic transmission, therefore, a model of this type of channel is used [20]. The channel is described:

$$ICa_{VGCC} = \bar{g}_{VGCC} r (V_{Pre} - E_{Ca}) \quad (11)$$

Where $\bar{g}_{VGCC}$ is the maximal channel conductance, r is the channel activation (a fraction of the voltage gates in the open state), V_{Pre} is the presynaptic membrane potential and E_{Ca} is the reversal potential of Ca^{2+}. Parameters are used from [20]. The channel activation is assumed to be instantaneous and voltage-dependent, therefore, the activation changes over time as the membrane potential changes and is described:

$$r = \left(1 + \exp\left(\frac{V_{Pre} + 0.01}{-0.06}\right)\right)^{-1}$$

D. Extracellular Diffusion Currents

The ECS diffusion current for each ionic species is generated by normal diffusion from the ECS to the global ECS along concentration gradients and is formulated using a standard ionic channel model, taken from [7], [12].

E. Astrocyte

The astrocyte model uses a complex morphology consisting of a perisynaptic process (sometimes known as the perisynaptic cradle (PsC)), with a relatively long and narrow astrocytic process that emanates from the astrocyte soma. Transmembrane proteins are only modelled at the cradle membrane and diffusion along the process is modelled as another signal pathway. The PsC is modelled using a three-dimensional morphology with the NCX on the outer membrane interacting with the GECS, and the PMCA on the inner membrane interacting with the ECS (see Fig. 1). This modelling methodology is used to show a complete Ca^{2+} signalling pathway from the GECS through the PsC into the ECS and finally, into the presynaptic neuron. Based on previous studies, the astrocyte membrane potential is held constant in this study at approximately —80mV [12], [13]. Most parameters are taken directly from the referenced models and the initial conditions of the system are calculated.

1) Total Currents

All the channels in the model are described in terms of current densities, therefore, the densities must be multiplied by the total surface area of the membrane to get the actual currents. The total astrocyte transmembrane currents are thus described:

$$ICa_{Ast} = (I_{PMCA} + ICa_{LPsC}) SA_{PsC}$$

$$INa_{Ast} = (INa_{NKAPsC} + INa_{EAAT} + INa_{LPsC}) SA_{PsC}$$

$$IK_{Ast} = (IK_{NKAPsC} + IK_{EAAT} + IK_{ir} + IK_{LPsC}) SA_{PsC}$$

Where I_{PMCA} is the current generated through the PMCA, Ix_{NKA} is the NKA current, Ix_{EAAT} is the EAAT current, Ix_{LPsC} is the background leak current, x is the ion under consideration, IK_{ir} is the Kir current and SA_{PsC} is the surface area of the PsC facing the ECS. The individual currents in the model are described in the following sections.

2) Ionic Channels

The ionic channels in the model are taken from the previous model [12], [13] and described only briefly here.

a) Na^+/K^+ ATPase

The NKA pumps both Na^+ and K^+ against their respective concentration gradients with a stoichiometry of $3Na^+$:$2K^+$ [21]. The current through the NKA is described in [12], [13], [22], and the same model is used for the astrocyte and neuronal cells.

b) Excitatory Amino-Acid Transporter

The excitatory amino-acid transporter (EAAT) is a transmembrane protein that transports excitatory amino-acids, like glutamate, across the cell membrane. Astrocytes have a high expression of EAAT proteins which are trafficked to the cellular membrane during synaptic activity to facilitate the rapid removal of glutamate from the synaptic environment [2]. The EAAT channels are activated when glutamate binds to the extracellular receptors and once activated, glutamate is cleared from the cleft almost instantly, ~3ms [23]. When the EAAT channel opens, glutamate is transported into the cell for approximately 30ms, while Na^+, K^+ and other ions like hydrogen (H^+) are free to flow along their concentration gradients [24]. The operation of the EAAT depends on concentrations of glutamate in the synaptic cleft, and because glutamate dynamics are not considered in the model, the time course of the channel opening and closing is sufficient. Therefore, the EAAT model assumes the binding of glutamate is instantaneous, the channel opens for 30ms and has a stoichiometry of $3Na^+$:$1K^+$ [24].

c) K^+ Inward Rectifying Channel

The Kir channel has a high affinity for K^+ and in normal conditions it allows K^+ to flow into the cell against its concentration gradient, hence the name inward rectifying. The direction K^+ flows down this channel is dependent on the concentrations of intracellular and extracellular K^+ and the membrane potential of the cell.

d) Na^+/Ca^{2+} Exchanger

The NCX is a secondary active transporter that uses the force generated by the large concentration gradient of Na^+ to extrude Ca^{2+} from the cell with a stoichiometry of $3Na^+$:$1Ca^{2+}$ [17]. The NCX is also known to extrude Na^+ while allowing Ca^{2+} into the cell during certain physiological conditions, this operation is known as "reverse mode". The NCX is known to reverse when the cell membrane potential hyperpolarises or the intracellular and extracellular concentrations change drastically [25]. As the astrocytic resting membrane potential is more hyperpolarised than the average neuronal resting potential (astrocyte resting potential ≈ —80mV), the NCX can readily enter reverse mode [26]. The NCX model is given in [12], [27]. The NCX is on the section of the PsC membrane facing the global ECS, shown in Fig. 1.

e) Plasma Membrane Ca^{2+} ATPase

The astrocytic PMCA is activated by any rise of $[Ca^{2+}]_i$ above resting concentration levels (~100nM in astrocytes). The current through the PMCA is modelled using standard Michaelis-Menten kinetics, similar to the model presented in [28], and is described:

$$I_{PMCA} = \bar{I}_{PM} \left(\frac{[Ca^{2+}]_{PsC}}{K_d + [Ca^{2+}]_{PsC}}\right) \quad (12)$$

Where $\bar{I}_{PM}$ is the maximum current generated through the PMCA, $[Ca^{2+}]_{PsC}$ is the intracellular Ca^{2+} concentration and K_d is the pump affinity, which also represents the concentration that the pump is operating at half its maximum velocity (usually ~200μM range) [18]. The maximum current through the PMCA, $\bar{I}_{PM}$, includes a conversion from maximal pump flux (V_{max} (mol/m^{2}s)) to current density (V_{max}*F (A/m^2)). The same model is used for the astrocyte and neuronal cells.

f) Leak Channels

The background leak channels are modelled as standard ohmic non-specific ion channels that allow ions to flow along their concentration gradients. The leak channels are given in [7], [12], and the channel conductances are calculated to obey Kirchoff's second law, i.e. all transmembrane currents must equal zero. The same model is used for the astrocyte and neuronal cells.

g) Process Currents

The ionic currents down the astrocytic process are modelled using the Poole-Frenkel effect [29]. This formula was previously used to model extremely thin astrocytic processes, ~100nm in diameter, showing the restriction of ionic diffusion and this is hypothesised to be due to deep potential energy wells along the process membrane [13].

TABLE I. MODEL PARAMETERS AND INITIAL CONDITIONS

Parameter	Value	Unit	Description	Ref.
dt	10×10^{-6}	s	Time step	
z_{Ca}	2	-	Valency of Ca^{2+}	
z_{Na}	1	-	Valency of Na^+	
z_K	1	-	Valency of K^+	
F	96485	C/mol	Faraday's constant	[30]
R	8.314	$J/mol.K$	Ideal gas constant	[30]
T	310	K	Absolute temperature	
Q	1.6022×10^{-19}	C	Elementary charge	[30]
$[Ca^{2+}]_{PsC}$	100×10^{-9}	M	Initial Ca^{2+} concentration in PsC	[6]
$[Na^+]_{PsC}$	15×10^{-3}	M	Initial Na^+ concentration in PsC	[6]
$[K^+]_{PsC}$	130×10^{-3}	M	Initial K^+ concentration in PsC	[6]
$[Ca^{2+}]_{Pre}$	50×10^{-9}	M	Initial Ca^{2+} concentration	[6]
$[Na^+]_{Pre}$	15×10^{-3}	M	Na^+ concentration	[6]
$[K^+]_{Pre}$	130×10^{-3}	M	K^+ concentration	[6]
$[Ca^{2+}]_{ECS}$	1.5×10^{-3}	M	Initial Ca^{2+} concentration in ECS	[6]
$[Na^+]_{ECS}$	135×10^{-3}	M	Initial Na^+ concentration in ECS	[6]
$[K^+]_{ECS}$	4×10^{-3}	M	Initial K^+ concentration in ECS	[6]
$[Ca^{2+}]_{GECS}$	1.5×10^{-3}	M	Ca^{2+} concentration in global ECS	[6]
$[Na^+]_{GECS}$	135×10^{-3}	M	Na^+ concentration in global ECS	[6]
$[K^+]_{GECS}$	4×10^{-3}	M	K^+ concentration in global ECS	[6]
Vol_{PsC}	1.855×10^{-17}	L	PsC compartment volume	Calc.
SA_{PsC}	1.41×10^{-13}	m^2	Inner PsC surface area	Calc.
SA_{PsCOut}	2.8274×10^{-13}	m^2	Outer PsC surface area	Calc.
CSA_{PF}	7.854×10^{-15}	m^2	Astrocyte process cross-sectional area	Calc.
l_{PF}	25×10^{-6}	m	Astrocyte process length	[6]
Vol_{Pre}	1×10^{-18}	L	Compartment volume	Calc.
SA_{Pre}	1.2723×10^{-13}	m^2	Compartment surface area	Calc.
Vol_{ECS}	2.0145×10^{-18}	L	Compartment volume	Calc.
SA_{ECS}	1.5715×10^{-14}	m^2	Diffusion surface area	Calc.
V_{Ast}	-0.0807	V	Astrocyte membrane potential	
V_{Rest}	-67.7×10^{-3}	V	Resting membrane potential	Calc.
I_{ext}	10	A/m^2	Externally applied stimulus	[19]
$\bar{g}_{VGCC}$	0.01	S/m^2	Maximal VGCC conductance	Calc. from [20]
r	4.5639×10^{-5}	-	Initial VGCC activation	Calc.
V_{max}	0.2×10^{-6}	mol/m^2s	Maximum PMCA flux	[18], [31]
$\bar{I}_{PM}$	0.0193	A/m^2	Maximum PMCA current	Calc.
K_d	0.2×10^{-6}	M	PMCA Ca^{2+} affinity	[18], [31]
g_{LPsCCa}	0.001398	S/m^2	Ca^{2+} leak conductance	Calc.
g_{LPsCNa}	0.9778	S/m^2	Na^+ leak conductance	Calc.
g_{LPsCK}	17.952	S/m^2	K^+ leak conductance	Calc.
g_{LPreCa}	0.013954	S/m^2	Ca^{2+} leak conductance	Calc.
g_{LPreNa}	2.3217	S/m^2	Na^+ leak conductance	Calc.
g_{LPreK}	1.0522	S/m^2	K^+ leak conductance	Calc.

TABLE II. REFERENCED IONIC CURRENT MODELS

Current	Description
Ix_{NKA}	Na^+/K^+ ATPase current can be found in [13]
Ix_{VG}	Voltage-gated current; can be found in [19]
Ix_L	Leak current; can be found in [7], [12]
$Ix_{ECSDiff}$	Extracellular diffusion current; can be found in [13]
Ix_{PF}	Astrocyte process current; can be found in [13]
Ix_{EAAT}	Excitatory amino-acid transporter current; can be found in [12]
IK_{ir}	K^+ inward rectifying current; can be found in [12]
Ix_{NCX}	Na^+/Ca^{2+} exchanger current; can be found in [12]

III. Results

The model was implemented using MATLAB 2019a 64-bit (Windows version) by Mathworks. This section will describe results of simulations with a total time of 100 seconds using a forward Euler numerical integration scheme with a fixed 10µs time step. During simulations, the neuronal compartment was stimulated from 10s to 40s, as this prolonged period of stimulus allows investigation of the effect of sustained neuronal activity on intracellular/extracellular ionic concentrations. The frequency of stimulation was changed for each simulation to compare the effects of higher frequency neuronal excitation. The linear stimulation frequencies used in the present work are 10Hz, 20Hz and 30Hz, and the results from each simulation are detailed in subsequent sections.

A. Astroglial Homeostatic Currents

The main pathways for astrocytic Ca^{2+} in the model are the NCX and the PMCA. The results in Fig. 2.B show Ca^{2+} entering the PsC through the NCX, while the PMCA begins to work harder to extrude the excess Ca^{2+}, seen in Fig. 2.A.

During the neuronal activity, the EAAT is activated by glutamate and the channel opens to allow Na^+ and K^+ flow along their gradients. The EAAT stays open for a relatively long period, ~30ms, and allows a significant influx of Na^+ and efflux of K^+. The EAAT stays open for approximately 30ms with the maximum flux rate being reached the instant a neuronal spike occurs. This relatively long duration current delivers approximately 1 mM of Na^+ into the cell over the entire time the channel is open, as well as leaking out K^+ at a rate of one third the Na^+ flux. The Na^+ current through the EAAT is the main driver of the astrocytic homeostatic response to neuronal activity, and the other Na^+ channels react to the perturbation of the cytosolic Na^+ ($[Na^+]_{PsC}$) caused by the EAAT Na^+ influx. The NKA works harder to maintain homeostasis, the NCX enters reverse mode to help extrude excess Na^+, the leak allows in fewer Na^+, while Na^+ also escapes the PsC through the astrocytic process. Even with Na^+ being extruded through the NKA, the NCX and the process, there is still enough Na^+ influx through the EAAT to cause the formation of a Na^+ microdomain in the PsC (not shown here).

The increase in $[Na^+]_{PsC}$ causes the NCX to flip from forward to reverse mode where it starts extruding Na^+ from the cell while simultaneously bringing Ca^{2+} into the cell. Cytosolic Ca^{2+} ($[Ca^{2+}]_{PsC}$) increases relatively quickly as a result of the NCX reversing and this causes the PMCA to start pumping excess Ca^{2+} out of the cell into the synaptic cleft. The PMCA and NCX are coupled; as the PMCA works harder to pump Ca^{2+} from the cell, the NCX is able to bring more Ca^{2+} into the cell because of the changing driving force. In this manner, the PMCA is capable of forcing the NCX to work harder while also preventing the formation of a large $[Ca^{2+}]_{PsC}$ microdomain. While the previous model showed the formation of a Ca^{2+} microdomain at the PsC [12], the results in Fig. 3.B show this microdomain is effectively translocated to the synaptic cleft. The NCX takes in Ca^{2+} from the GECS and starts to form a local microdomain on the order of micromolars. At the same time, the PMCA begins to remove $[Ca^{2+}]_{PsC}$ and this limits the Ca^{2+} microdomain to an order of nanomolars. Excess $[Ca^{2+}]_{PsC}$ flows down the process at a slow rate (due to the restricted ionic model used [13]), shown in Fig. 2.C. The Ca^{2+} leak channel, seen in Fig 2.D, reacts according to the change in electrochemical driving force from the changing intracellular/extracellular concentrations.

B. Ionic Concentrations

The concentrations of Na^+, K^+ and Ca^{2+} are captured in three separate compartments; the presynaptic neuron (Pre), the astrocytic perisynaptic complex (PsC) and the synaptic cleft (ECS). The dynamics of concentrations in each compartment

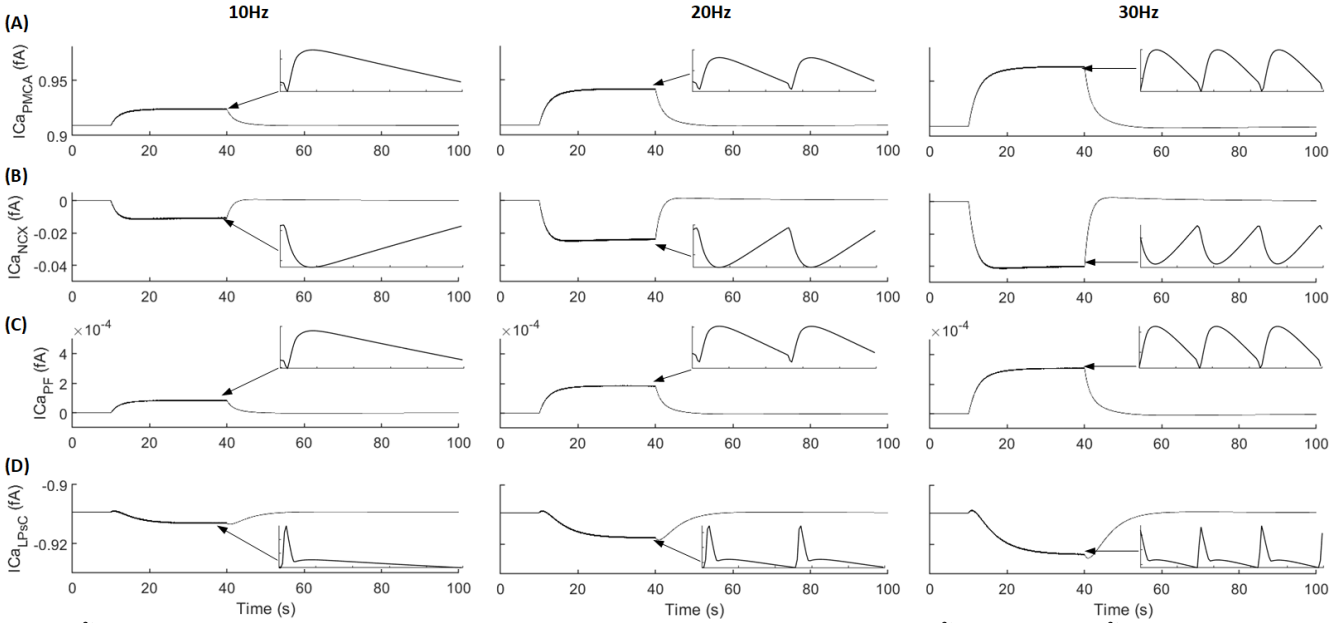

Fig. 2. Ca^{2+} currents in the PsC. (A) PMCA current. This is an outward current driven by the change in $[Ca^{2+}]_{PsC}$. (B) NCX Ca^{2+} current. The increase in $[Na^+]_{PsC}$ causes the NCX to reverse, allowing an influx of Ca^{2+}. At rest there is no current through the NCX but, during neuronal excitability, the Ca^{2+} component of the NCX current becomes an inward current that reaches up to ~0.04fA. (C) Process Ca^{2+} current. This is zero at rest and becomes an outward current when $[Ca^{2+}]_{PsC}$ rises. The maximum current down the process is ~3*10^{-4}fA at 30Hz. (D) Ca^{2+} leak current. This is an inward current that follows the changing electrochemical driving force. The inset plots detail 100ms from t = 39s to t = 39.1s.

are intrinsically tied together, for example, if Na^+ levels drop in ECS then there is fewer Na^+ able to enter Pre or PsC. The Pre and PsC compartments can sense concentration changes in the ECS compartment because they are interfacing directly with the synaptic cleft. The astrocytic NCX is an exception to this rule as it is interfacing with the global ECS (GECS). The concentrations are held constant in the astrocyte soma and the GECS because these compartments are assumed sufficiently large enough to be infinite relative to the compartments being studied. Ca^{2+} concentration results in Fig. 3.A and 3.B show the Ca^{2+} microdomain reported previously in [12] has been translocated from the PsC to the ECS. The PMCA keeps $[Ca^{2+}]_{PsC}$ low, ~10nM above resting at 30Hz, while $[Ca^{2+}]_{ECS}$ rises approximately 0.5mM at 30Hz. The massive difference in concentration changes is due to the compartment volumes; the PsC is approximately 9 times larger than the ECS (see Table I for calculated compartment volumes).

IV. Discussion

When glutamate is released from the neuron during excitable periods, the astrocyte begins taking homeostatic action by clearing the glutamate and taking Na^+ from the synaptic cleft. This clears the cleft for further synaptic transmission but also leads to excess Na^+ in the astrocyte which consequently forces the NCX to reverse and allow Ca^{2+} into the astrocyte. The results from the simulations show that even in the absence of an endoplasmic reticulum region or any other intracellular Ca^{2+} stores, and only through the reversal of the NCX, the perisynaptic astrocyte can still generate local Ca^{2+} microdomains large enough to supply the synaptic cleft with ample Ca^{2+} to enhance synaptic transmission during prolonged neuronal activity, which may be important for processes involving Ca^{2+} such as synaptic plasticity. Furthermore, Ca^{2+} is thought to be vital for increasing the probability of synaptic neurotransmitter release, therefore, if the perisynaptic astrocyte were to retract from the synapse or channels in the astrocyte failed, such as the PMCA or NCX, this would have negative consequences for synaptic transmission and neural circuits. These findings provide an alternative to the highly debated gliotransmission theory.

The model results also demonstrate that astrocytic concentrations of different ionic species are functionally coupled via specific active transporters and channels, as expected. For example, the concentrations of Ca^{2+} and Na^+ are coupled in the astrocyte due to the NCX exchanging both ionic species. Na^+ and K^+ are also coupled by the NKA pump. This means that the ionic concentrations are inter-dependent on each other to maintain homeostasis. From this inter-dependent relationship, Ca^{2+} and K^+ are indirectly coupled through the Na^+ concentration. For example, our results show that as $[Ca^{2+}]_{PsC}$ increases the NCX reverses an extrudes Na^+, which makes the NKA work at a slower rate to extrude Na^+, and therefore, K^+ is being replenished at a slower rate. Effectively, the rise in $[Ca^{2+}]_{PsC}$ causes a change in Na^+ behaviour which in turn causes a change in K^+ behaviour.

V. Conclusion

Using a five-compartment conductance-based mathematical model we found prolonged neuronal activity causes the reversal of the NCX in the perisynaptic astrocyte which in turn causes the synaptic cleft to be supplied with Ca^{2+} from the astrocyte. The Ca^{2+} concentration in the semi-

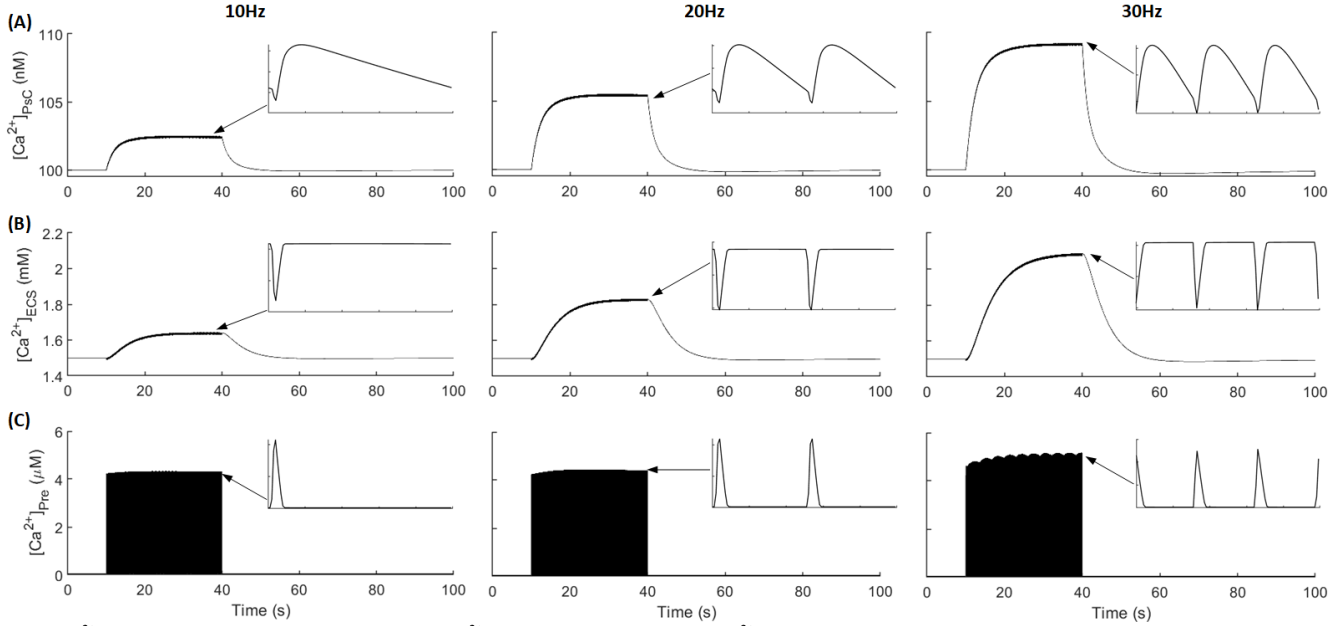

Fig. 3. Ca^{2+} concentrations in all compartments. (A) Ca^{2+} concentration in the PsC ($[Ca^{2+}]_{PsC}$). A local microdomain forms in the PsC, reaching up to between 3-10nM above the resting concentration. The $[Ca^{2+}]_{PsC}$ concentration fluctuations (inset plot) are due to the NCX and PMCA working against each other, with the NCX bringing Ca^{2+} in to the cell and the PMCA removing from the cell to maintain homeostasis. Ca^{2+} homeostasis is achieved ~10 seconds after neuronal activity ceases. (B) Ca^{2+} concentration in the ECS ($[Ca^{2+}]_{ECS}$). A significant build up of Ca^{2+} occurs due to the semi-isolated nature of the ECS along with Ca^{2+} extrusion from the astrocyte; between ~0.1-0.7mM. $[Ca^{2+}]_{ECS}$ is the primary source of Ca^{2+} to the presynaptic neuron and returns to resting concentration after ~60 seconds. (C) Ca^{2+} concentration in the presynaptic neuron ($[Ca^{2+}]_{Pre}$). The rise in $[Ca^{2+}]_{Pre}$ is due to the opening of the VGCC, reaching up to between 4-5μM. This is a drastic change in a relatively short period of time but the action of the PMCA returns $[Ca^{2+}]_{Pre}$ to resting concentration in a matter of milliseconds. The inset plots detail 100ms from t = 39s to t = 39.1s.

isolated cleft increased quite significantly in a relatively short period of time; ~0.5mM rise in 30 seconds. This level of Ca^{2+} should be felt by the neuron and synaptic transmission will be affected as a result. The scale of the model is extremely small, e.g. the astrocytic process diameter is 100 nm, and this will have implications when testing the model experimentally. This means the model may not be validated by experiments for a number of years, although it can still be used to make predictions and steer future work in this area.

This computational study will form the basis for future work on the effects of astrocytes on synaptic plasticity, both long and short term types. Ca^{2+} has been implicated in both types of synaptic plasticity; it affects short-term plasticity by affecting the probability of neurotransmitter release at the presynaptic terminal and it affects long-term plasticity by helping to increase ion channel conductances on the postsynaptic membrane. Ca^{2+} also contributes to the insertion of ion channels in the postsynaptic membrane, another instance of how Ca^{2+} affects long-term plasticity. The astrocytic influences on synaptic plasticity, at both the presynaptic and postsynaptic neurons, will be investigated using a computational approach, which will lead to a more complete understanding of the underlying biological processes involved in synaptic plasticity and ultimately better computational models of learning which can be applied to networks of spiking neurons.

REFERENCES

[1] A. H. Cornell-Bell, S. M. Finkbeiner, M. S. Cooper, and S. J. Smith, "Glutamate induces calcium waves in cultured astrocytes: long-range glial signaling.," *Science*, vol. 247, no. 4941, pp. 470–3, Jan. 1990.

[2] A. Verkhratsky and A. Butt, *Glial Neurobiology*. Chichester, UK: John Wiley & Sons, Ltd, 2007.

[3] A. Verkhratsky and M. Nedergaard, "Astroglial cradle in the life of the synapse," *Philos. Trans. R. Soc. B Biol. Sci.*, vol. 369, no. 1654, pp. 20130595–20130595, Sep. 2014, doi: 10.1098/rstb.2013.0595.

[4] E. R. Kandel, J. H. Schwartz, T. M. Jessell, S. A. Siegelbaum, and A. J. Hudspeth, *Principles of Neural Science*, Fifth. McGraw-Hill, 2012.

[5] M. Nedergaard and A. Verkhratsky, "Artifact versus reality-How astrocytes contribute to synaptic events," *Glia*, vol. 60, no. 7, pp. 1013–1023, Jul. 2012, doi: 10.1002/glia.22288.

[6] A. Verkhratsky and M. Nedergaard, "Physiology of Astroglia," *Physiol. Rev.*, vol. 98, no. 1, pp. 239–389, Jan. 2018, doi: 10.1152/physrev.00042.2016.

[7] J. Keener and J. Sneyd, *Mathematical Physiology*, vol. 8/1. New York, NY: Springer New York, 2009.

[8] C. R. Rose, L. Felix, A. Zeug, D. Dietrich, A. Reiner, and C. Henneberger, "Astroglial Glutamate Signaling and Uptake in the Hippocampus," *Front. Mol. Neurosci.*, vol. 10, Jan. 2018, doi: 10.3389/fnmol.2017.00451.

[9] M. D. Haustein, S. Kracun, X.-H. Lu, T. Shih, O. Jackson-Weaver, X. Tong, *et al.*, "Conditions and Constraints for Astrocyte Calcium Signaling in the Hippocampal Mossy Fiber Pathway," *Neuron*, vol. 82, no. 2, pp. 413–429, Apr. 2014, doi: 10.1016/j.neuron.2014.02.041.

[10] R. L. Rungta, L.-P. Bernier, L. Dissing-Olesen, C. J. Groten, J. M. LeDue, R. Ko, *et al.*, "Ca 2+ transients in astrocyte fine processes occur via Ca 2+ influx in the adult mouse hippocampus," *Glia*, vol. 64, no. 12, pp. 2093–2103, Dec. 2016, doi: 10.1002/glia.23042.

[11] A. Derouiche, E. Anlauf, G. Aumann, B. Mühlstädt, and M. Lavialle, "Anatomical aspects of glia–synapse interaction: the perisynaptic glial sheath consists of a specialized astrocyte compartment," *J. Physiol.*, vol. 96, no. 3–4, pp. 177–182, May 2002, doi: 10.1016/S0928-4257(02)00004-9.

[12] J. J. Wade, K. Breslin, K. Wong-Lin, J. Harkin, B. Flanagan, H. Van Zalinge, *et al.*, "Calcium Microdomain Formation at the Perisynaptic Cradle Due to NCX Reversal: A Computational Study," *Front. Cell. Neurosci.*, vol. 13, 2019, doi: 10.3389/fncel.2019.00185.

[13] K. Breslin, J. J. Wade, K. Wong-Lin, J. Harkin, B. Flanagan, H. Van Zalinge, *et al.*, "Potassium and sodium microdomains in thin astroglial processes: A computational model study," *PLOS Comput. Biol.*, vol. 14, no. 5, p. e1006151, May 2018, doi: 10.1371/journal.pcbi.1006151.

[14] A. Araque, V. Parpura, R. P. Sanzgiri, and P. G. Haydon, "Tripartite synapses: glia, the unacknowledged partner.," *Trends Neurosci.*, vol. 22, no. 5, pp. 208–15, May 1999.

[15] I. Savtchouk and A. Volterra, "Gliotransmission: Beyond Black-and-White," *J. Neurosci.*, vol. 38, no. 1, pp. 14–25, Jan. 2018, doi: 10.1523/JNEUROSCI.0017-17.2017.

[16] T. A. Fiacco and K. D. McCarthy, "Multiple Lines of Evidence Indicate That Gliotransmission Does Not Occur under Physiological Conditions," *J. Neurosci.*, vol. 38, no. 1, pp. 3–13, Jan. 2018, doi: 10.1523/JNEUROSCI.0016-17.2017.

[17] A. Verkhratsky, M. Trebak, F. Perocchi, D. Khananshvili, and I. Sekler, "Crosslink between calcium and sodium signalling.," *Exp. Physiol.*, vol. 103, no. 2, pp. 157–169, Feb. 2018, doi: 10.1113/EP086534.

[18] M. Brini and E. Carafoli, "The Plasma Membrane Ca2+ ATPase and the plasma membrane Sodium Calcium exchanger cooperate in the regulation of cell Calcium," *Cold Spring Harb. Perspect. Biol.*, vol. 3, no. 2, pp. 1–15, 2011, doi: 10.1101/cshperspect.a004168.

[19] A. L. Hodgkin and A. F. Huxley, "A quantitative description of membrane current and its application to conduction and excitation in nerve.," *J. Physiol.*, vol. 117, no. 4, pp. 500–44, Aug. 1952, doi: 10.1007/BF02459568.

[20] M. Riz, M. Braun, and M. G. Pedersen, "Mathematical Modeling of Heterogeneous Electrophysiological Responses in Human β-Cells," *PLoS Comput. Biol.*, vol. 10, no. 1, 2014, doi: 10.1371/journal.pcbi.1003389.

[21] C. R. Rose and A. Verkhratsky, "Principles of sodium homeostasis and sodium signalling in astroglia.," *Glia*, vol. 64, no. 10, pp. 1611–27, 2016, doi: 10.1002/glia.22964.

[22] G. Halnes, I. Østby, K. H. Pettersen, S. W. Omholt, and G. T. Einevoll, "Electrodiffusive Model for Astrocytic and Neuronal Ion Concentration Dynamics," *PLoS Comput. Biol.*, vol. 9, no. 12, p. e1003386, Dec. 2013, doi: 10.1371/journal.pcbi.1003386.

[23] Y. Zhou and N. C. Danbolt, "GABA and glutamate transporters in brain," *Frontiers in Endocrinology*, vol. 4. 2013, doi: 10.3389/fendo.2013.00165.

[24] C. Grewer, A. Gameiro, and T. Rauen, "SLC1 glutamate transporters," *Pflugers Archiv European Journal of Physiology*, vol. 466, no. 1. pp. 3–24, 2014, doi: 10.1007/s00424-013-1397-7.

[25] A. Volterra, N. Liaudet, and I. Savtchouk, "Astrocyte Ca2+ signalling: An unexpected complexity," *Nature Reviews Neuroscience*, vol. 15, no. 5. pp. 327–335, 2014, doi: 10.1038/nrn3725.

[26] A. J. Hansen, "Effect of anoxia on ion distribution in the brain," *Physiol. Rev.*, vol. 65, no. 1, pp. 101–148, Jan. 1985, doi: 10.1152/physrev.1985.65.1.101.

[27] F. Gabbiani and S. J. Cox, *Mathematics for Neuroscientists*. Elsevier, 2010.

[28] C. H. Luo and Y. Rudy, "A Dynamic Model of the Cardiac Ventricular Action Potential," *Circ. Res.*, vol. 74, no. 6, pp. 1071–1096, 1994.

[29] J. Frenkel, "On pre-breakdown phenomena in insulators and electronic semi-conductors," *Physical Review*, vol. 54, no. 8. pp. 647–648, 1938, doi: 10.1103/PhysRev.54.647.

[30] NIST, "The NIST Reference on Constants, Units, and Uncertainty," 2019. [Online]. Available: https://physics.nist.gov/cuu/Constants/index.html. [Accessed: 18-Sep-2019].

[31] D. Sterratt, B. Graham, A. Gillies, and D. Willshaw, *Principles of Computational Modelling in Neuroscience*. 2011.